



**Calhoun: The NPS Institutional Archive**  
**DSpace Repository**

---

NPS Scholarship

Publications

---

2005-06

# The influence of friction stir processing parameters on microstructure of as-cast NiAl bronze

Oh-Ishi, Keiichiro; McNelley, Terry R.

Minerals, Metals & Materials Society

---

K. Oh-Ishi, T.R. McNelley, "The influence of friction stir processing parameters on microstructure of as-cast NiAl bronze," Metallurgical and Materials Transactions A, v.36A,(2005), pp.1575-1585

<https://hdl.handle.net/10945/55340>

---

This publication is a work of the U.S. Government as defined in Title 17, United States Code, Section 101. Copyright protection is not available for this work in the United States.

*Downloaded from NPS Archive: Calhoun*



Calhoun is the Naval Postgraduate School's public access digital repository for research materials and institutional publications created by the NPS community. Calhoun is named for Professor of Mathematics Guy K. Calhoun, NPS's first appointed -- and published -- scholarly author.

**Dudley Knox Library / Naval Postgraduate School**  
**411 Dyer Road / 1 University Circle**  
**Monterey, California USA 93943**

<http://www.nps.edu/library>

# The Influence of Friction Stir Processing Parameters on Microstructure of As-Cast NiAl Bronze

KEIICHIRO OH-ISHI and TERRY R. McNELLEY

The influence of friction stir processing (FSP) parameters on the evolution of microstructure in an equilibrium-cooled, as-cast NiAl bronze (NAB) material was evaluated by optical microscopy (OM) and transmission electron microscopy (TEM) methods. A threaded pin tool was employed and tool rotation and traversing rates were varied in order to examine the spatial variation of stir zone microstructures in relation to FSP parameters. For processing at low rotation and traversing rates, the microstructure throughout the stir zone consists of elongated and banded grains of the primary  $\alpha$  and transformation products of the  $\beta$  phase. Such microstructures reflect severe deformation at temperatures up to  $\sim 900$  °C in the  $\alpha + \beta$  two-phase region for this NAB material. Increasing rotation and traversing rates, coarse Widmanstätten  $\alpha$  near the surface in contact with the tool became apparent. The appearance of this constituent reflects nearly complete transformation to  $\beta$  during FSP with peak temperatures of  $\sim 1000$  °C. Also, complex stir zone flow patterns, often referred to as onion ring structures, become distinct in the mid regions of the stir zones as rotation and traversing rates increase. Schematic representations illustrating the effect of FSP parameters on thermal cycles at various locations in stir zones were prepared based on microstructure observations. Thus, processing at higher rotation and traversing rates results in higher peak temperatures near the surface in contact with the tool but also in steeper temperature gradients when compared to lower rotation and traversing rates.

## I. INTRODUCTION

FRICITION stir processing (FSP) is a solid-state technique that can provide localized modification and control of microstructure in the near-surface regions of a deformable metal.<sup>[1,2,3]</sup> The concept of FSP is relatively simple: a cylindrical, wear-resistant tool having a larger-diameter shoulder and a concentric smaller-diameter pin is rotated while the pin is forced into the surface of the material. The pin penetrates until the tool shoulder comes into contact with the surface and the tool is then traversed along a path to process the region of interest. Frictional and adiabatic heating due to a combination of sliding and sticking conditions at the workpiece surface in contact with the tool led to localized heating and softening and to steep gradients in strain, strain rate, and temperature within a localized stir zone surrounding the pin. The tool shoulder acts to constrain upward displacement of the material in the stir zone, while severe plastic deformation in the stir zone results in movement of material about the pin.

The localized thermomechanical cycle of FSP homogenizes and refines stir zone microstructures, leading to improved material properties in the processed layers. The FSP is an adaptation of friction stir welding (FSW) technology and has been applied to achieve localized microstructure modification in wrought and powder metallurgy materials as well as cast metals.<sup>[4-11]</sup> For example, in wrought AA7075, FSP has been used to generate highly refined grains that support high-strain-rate superplasticity.<sup>[4,5,6]</sup> The tech-

nique has also been used to bond surface layers of composite material, 50 to 200  $\mu\text{m}$  in thickness and containing uniformly distributed SiC particles, to an aluminum alloy substrate.<sup>[2]</sup> The resulting material exhibited significant surface hardening. Improved microstructures and properties in nanophase aluminum alloys have also been attained by FSP.<sup>[7]</sup>

For cast metals, FSP can homogenize the as-cast microstructures and redistribute inclusions as well as close porosity in the stir zone. The processed surface layers are effectively converted from a cast to a wrought condition in the absence of macroscopic shape change and so FSP represents a means for surface modification and hardening of cast components. Processing of as-cast AA356 (nominally Al-7 wt pct Si) by FSP resulted in redistribution of the eutectic Si located in interdendritic regions of as-cast material as equiaxed particles in processed material, while porosity was eliminated in the stir zone.<sup>[3]</sup> Nevertheless, bandlike or ringlike features consisting of layered regions having either finer or coarser Si particles were observed in transverse sections through stir zones. The extent of improvements in tensile properties depended on FSP parameters, *i.e.*, tool design, rotation rate, and traversing speed. Microstructures involving bandlike variations in grain size, constituent distribution, or inclusion content have all been documented in investigations into both FSW and FSP and such features may affect the resulting mechanical properties.<sup>[3,12-15]</sup>

The application of FSP to as-cast NiAl bronze (NAB) alloys has also been shown to provide microstructure refinement and elimination of casting porosity.<sup>[16]</sup> These alloys are widely used for marine components that often involve thick sections. The slow cooling rates (typically  $10^{-3}$  to  $10^{-2}$  °C s<sup>-1</sup>) in such circumstances may result in reduced properties, and so FSP represents a method for selectively strengthening such components. The physical metallurgy of NAB alloys is complex. The constitution and transformation characteristics of these materials have already been described in detail<sup>[17-22]</sup>

---

KEIICHIRO OH-ISHI, Postdoctoral Research Associate, and TERRY R. McNELLEY, Professor of Materials Science, are with the Center for Materials Science, Department of Mechanical and Astronautical Engineering, Naval Post Graduate School, Monterey, CA 93943-5146. Contact email: tmcnelley@nps.edu

Manuscript October 21, 2004.

and reviewed recently.<sup>[16]</sup> Briefly, NABs are quaternary Cu-Al-Ni-Fe alloys; the UNS95800 alloy of interest in the present work is nominally Cu-9Al-5Ni-4Fe (compositions in weight percent).<sup>[23]</sup> During cooling at a nominal rate of  $\sim 10^{-3} \text{ }^\circ\text{C s}^{-1}$ , the cast metal solidifies as a single-phase  $\beta$  bcc solid solution and cools as  $\beta$  until about 1030 °C. Below this temperature, the primary  $\alpha$  fcc terminal solid solution begins to form in the  $\beta$  with a Widmanstätten morphology. At 930 °C, a globular precipitate,  $\kappa_{ii}$ , which is nominally  $\text{Fe}_3\text{Al}$  and has a  $\text{DO}_3$  structure, begins to form in the remaining  $\beta$ . The globular  $\kappa_{ii}$  precipitates may reach sizes of 20 to 30  $\mu\text{m}$ . Upon cooling below 860 °C, a finer  $\text{Fe}_3\text{Al}$  precipitate,  $\kappa_{iv}$ , begins to form in the primary  $\alpha$ . Finally, the volume of  $\beta$  continues to decrease until a eutectoid reaction,  $\beta \rightarrow \alpha + \kappa_{iii}$ , takes place at 800 °C. The  $\kappa_{iii}$  is nominally NiAl having a B2 structure. Thus, following such equilibrium cooling, the microstructure consists of the primary  $\alpha$ , which contains a fine dispersion of the  $\kappa_{iv}$ , and a eutectoid constituent,  $\alpha + \kappa_{iii}$ . The coarse, globular  $\kappa_{ii}$  phase is dispersed in the eutectoid constituent.

The effects of FSP on the microstructure of an equilibrium-cooled NAB material have been evaluated in a recent article.<sup>[16]</sup> A single tool design and one set of FSP parameters were considered in a detailed study of phase transformations in this NAB material. The selected parameters were deemed representative of FSP and resulted in stir zone peak temperatures in the range of 800 °C to 900 °C, with subsequent cooling rates that were estimated to be  $\sim 10^0 \text{ }^\circ\text{C s}^{-1}$ . Phase transformations during cooling of NAB materials are strongly dependent on the initial annealing temperature and subsequent cooling rates. The analysis revealed that the severe concurrent deformation during the heating of FSP tended to accelerate reactions such as the reversion of the eutectoid  $\alpha + \kappa_{iii} \rightarrow \beta$ . This reaction took place in regions where the peak temperature exceeded 800 °C. The cooling rates in processed material resulted in various nonequilibrium transformation products of the  $\beta$ , which included mixtures of Widmanstätten  $\alpha$ , bainite, and martensite. Peak temperatures at various locations in the stir zone could be estimated based on these observations; this is useful because direct measurement of temperature in such locations is infeasible. The current investigation was initiated in order to assess the role of FSP parameters in the evolution of the microstructure in as-cast NAB materials.

## II. EXPERIMENTAL PROCEDURES

The material examined in this investigation conforms to the composition specification for UNS95800 NAB. This specification was included in a previous report,<sup>[16]</sup> and the composition data for the alloy of interest here are also provided in Table I. The FSP was accomplished at Rockwell Scientific Company (Thousand Oaks, CA) with tools machined from MP159, an alloy having a nominal composition of 25Ni-36Co-19Cr-9Fe-7Mo-3Ti (wt pct). Details of the tool design were also given previously;<sup>[16]</sup> briefly, the tools were machined to have a shoulder diameter of 23.8 mm, pin diameter of 7.95 mm, and pin depth of 6.65 mm. In addition, the pin had a spiral groove. In the present investigation, as-cast NAB material was processed using four different combinations of tool rotation and tra-

**Table I. Composition Data for the UNS95800 NAB Alloy Examined in this Investigation**

| Element | Cu   | Al   | Ni   | Fe   | Mn   | Si   | Pb     |
|---------|------|------|------|------|------|------|--------|
| Alloy   | 81.2 | 9.39 | 4.29 | 3.67 | 1.20 | 0.05 | <0.005 |

**Table II. Processing Parameters for the Tool Employed in this Study**

| Process Parameters                    | FSP 514 | FSP 516 | FSP 520 | FSP 528 |
|---------------------------------------|---------|---------|---------|---------|
| Rotation rate (rpm)                   | 600     | 800     | 1000    | 1200    |
| Traversing rate (mm m <sup>-1</sup> ) | 25.4    | 152     | 203     | 406     |

versing rates, as summarized in Table II.<sup>[24]</sup> Each of these processes involved a traverse approximately 200 mm in length. The sample designators are only serial numbers. In all cases, the tool was inclined  $\sim 3$  deg opposite the direction of tool advance (the  $x$  direction) and the FSP was conducted under  $x$ -axis displacement rate control.<sup>[16,24]</sup> At the highest rotation and traversing rates, the pin deformed in the initial stages of processing and became compressed by 1 to 2 mm, with a varying pin diameter. No tool erosion or transfer of tool material to the work piece was observed; nevertheless, tools have subsequently been machined from Densimet, a powder metallurgy W-Ni material, in order to eliminate tool deformation.

Microscopy methods have also been described previously.<sup>[16]</sup> Briefly, samples for microscopy were prepared by sectioning on a transverse plane so that the direction of tool advance was aligned into the plane of the section. The sections were located approximately at the midpoint of traverses where FSP appeared to be at a steady state. Optical microscopy (OM) involved standard preparation methods; etching used a two-step process involving immersion for 1 to 2 seconds in a solution of 40 mL water-40 mL ammonium hydroxide-2 mL hydrogen peroxide (30 pct), and rinsing in water, followed by immersion for 1 to 2 seconds in a solution of 60 mL water-30 mL phosphoric acid-10 mL hydrogen peroxide. Etched samples were examined using bright-field (BF) illumination in a JENAPHOT\* 2000 equipped with a digital

\*JENAPHOT is a trademark of Carl Zeiss, Oberkochen, Germany.

imaging system. Transmission electron microscopy (TEM) was accomplished with a TOPCON\*\* 002B instrument

\*\*TOPCON is a trademark of Topcon America Corp., Paramus, NJ.

operating at 200 kV. Samples for TEM examination were obtained by first sectioning with a low-speed diamond saw to obtain a transverse slice through the stir zone of processed material. Then, disks 3 mm in diameter and having normal directions parallel to the travel direction were thinned to perforation by electropolishing using a 33 pct nitric acid-67 pct methanol solution initially cooled to  $-25 \text{ }^\circ\text{C}$ ; ion milling using a HITACHI\*\*\* E-300 ion mill operating at 4 kV for

\*\*\*HITACHI, Ltd., Tokyo, Japan.

$\sim 1$  hour was employed with selected samples.

### III. RESULTS

#### A. Microstructure Examination with OM

##### 1. Transverse cross section of stir zone

Figure 1 shows montages of optical micrographs illustrating transverse sections of the stir zones for samples FSP 514, 520, and 528. A corresponding montage for sample FSP 516 has appeared previously.<sup>[16]</sup> For all of these images, the direction of tool advance is into the page and so the advancing side is to the right while the retreating side is to the left. In addition, the profile of the upper sample surface in contact with the tool is visible toward the upper side of each montage. The width of the stir zone at the surface of the material in contact with the tool shoulder is the same for all of these processing conditions. The FSP 514 stir zone has the largest apparent area among these samples, which reflects deeper penetration of the frictional and adiabatic heating at the lower tool rotation and travel rates (Table II). This is most apparent on both the advancing and retreating sides, which are regions affected mainly by the shoulder. Comparison of these montages clearly reveals that the stir zone depth under the tool shoulder decreases with increasing tool rotation and travel rates. Near the center, stir zone depths are dominated by the pin length; the decreasing stir zone depth with increasing tool rotation and travel rates mainly reflects tool shape change due to compressive deformation of the pin. There was no evidence of tool erosion and transfer of tool material to the stir zone.

A bandlike structure is evident throughout the stir zone of FSP 514. This structure consists of alternating light- and

dark-etched phases that are elongated and generally aligned in a horizontal direction. We have reported previously that the lighter and darker phases are the primary  $\alpha$  phase and the products of  $\beta$  transformation during cooling, respectively.<sup>[16]</sup> The FSP 520 and 528 both exhibit this structure but only in block- or needlelike regions that extend horizontally from a location under the tool shoulder on the retreating side inward across the stir zone. The primary  $\alpha$  and  $\beta$  transformation products are both finer and less distinct in these regions than in FSP 514 (and in FSP 516, as well<sup>[16]</sup>). A more complicated pattern of material flow is apparent in the central regions of the stir zones in FSP 520 and 528. A swirl pattern, or so-called “onion-ring structure,”<sup>[25]</sup> is apparent for these latter conditions; such a pattern reflects displacement fields involving vertical as well as horizontal components during deformation of the material.<sup>[26]</sup>

In addition, the thermomechanically affected zone (TMAZ), which is the region outside the stir zone that experiences mainly heating during FSP, is most extensive after FSP at the lowest tool rotation and travel rates. For all of these processing conditions, the boundary between the stir zone and TMAZ is always more distinct on the advancing side and less so on the retreating side, and a comparison among these conditions indicates complex grain deformation patterns within the TMAZ in the vicinity of the stir zone–TMAZ interface. Under the tool on the advancing side, grain shape distortion suggests local displacements along the interface and, in some locations on the advancing side, flow upward toward the tool shoulder.

The interface between the stir zone and the TMAZ is generally indistinct on the retreating side. In some locations (such as those indicated by arrows in Figures 1(b) and (c)), grain flow patterns on the retreating side suggest a gradual transition from the TMAZ to the stir zone, and the block- or needlelike regions of primary  $\alpha$  and the  $\beta$  transformation products are formed from TMAZ material that is drawn into the stir zone from the retreating side as the tool advances. These grain flow patterns comprise a dark-etching constituent that is the bainitic or martensitic transformation products of  $\beta$ , as well as the primary  $\alpha$ . In the TMAZ, these constituents reflect the eutectoid reversion reaction  $\alpha + \kappa_{iii} \rightarrow \beta$  accompanied by, at most, small deformations, while these constituents become progressively elongated in a horizontal direction as the material deforms into these regions. Altogether, these observations suggest that the gradients in strain, strain rate, and temperature are steeper on the advancing side than on the retreating side. These steeper gradients on the advancing side reflect that the direction of tool travel is parallel to the tool surface tangential velocity on the advancing side and antiparallel to it on the retreating side. Other effects that are not apparent at the level of magnification in Figure 1 may include the break up and refinement of the various  $\kappa$  phases that remain undissolved during processing. Because the advancing side is subjected to larger strains and strain rates than the retreating side, spheroidization and break up of these phases may occur more readily on the advancing side.

##### 2. Various locations within the stir zone

The variation in microstructure within the stir zone depends on process parameters. Figure 2 shows higher magnification micrographs for regions 1 and 2 in FSP 514; the locations of these regions within the stir zone are indicated in Figure 1(a). Figures 2(a) and (b) represent upper and lower

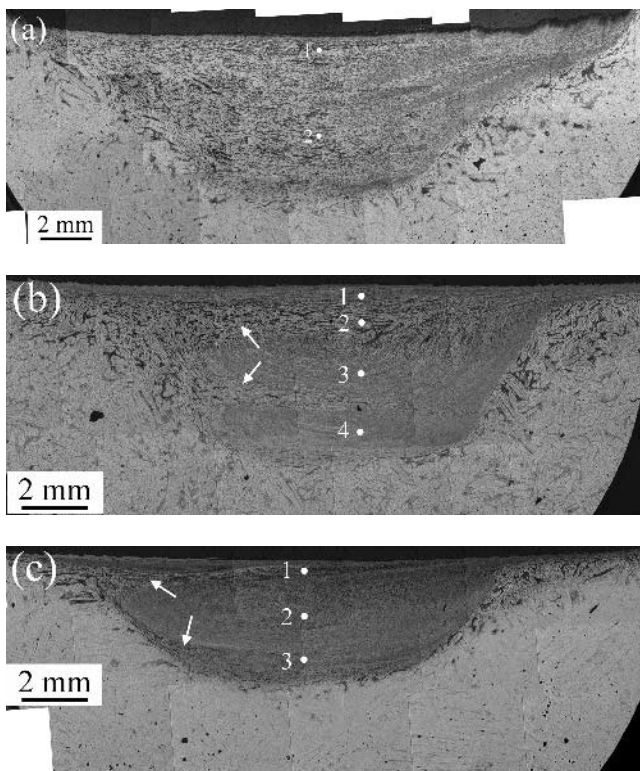


Fig. 1—Optical micrographs of transverse sections of the stir zones for (a) FSP 514, (b) FSP 520, and (c) FSP 528. The advancing side is to the right side, and the retreating side is to the left side. The number points indicate the locations of the regions observed at higher magnification.

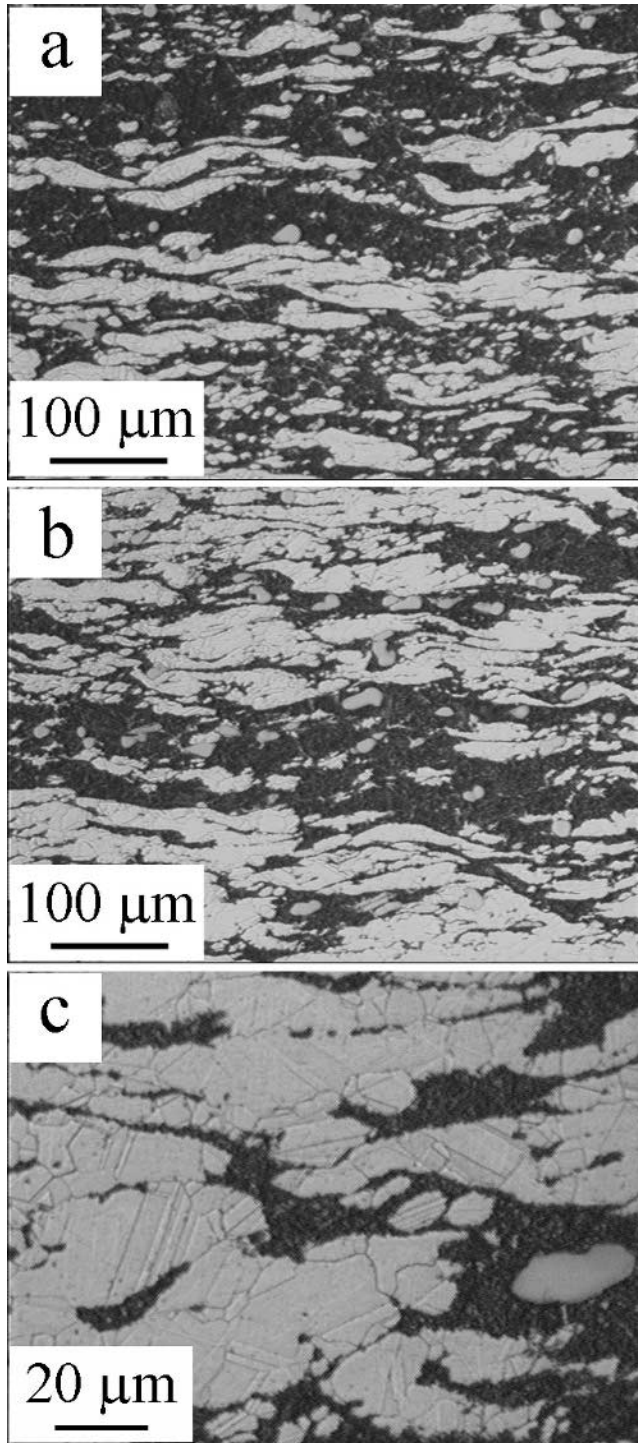


Fig. 2—Higher magnification optical micrographs for (a) upper and (b) lower regions along the centerline of the stir zone in FSP 514, corresponding to regions 1 and 2 in Fig. 1(a), respectively. (c) Annealing twins are apparent in the  $\alpha$  grains at still higher magnification in region 2.

regions along the centerline of the stir zone, respectively. Elongated and banded structures consisting of  $\alpha$  phase (light etching) and prior  $\beta$  phase (dark etching) appear clearly in both regions, although the relative amount of the  $\beta$  constituent appears to be greater near the sample surface. In both regions, these constituents are elongated in the hori-

zontal direction. In Figure 2(c), annealing twins are apparent in the primary  $\alpha$  grains when region 2 is examined at higher magnification. The presence of such twins in primary  $\alpha$  was also documented by TEM of FSP 516.<sup>[16]</sup>

Figure 3 illustrates the variation in microstructure for different regions along a traverse through the center of the stir zone in FSP 520 (Figure 1(b)). Figure 3(a) is from the location nearest the surface, region 1 in Figure 1(b), and shows distinct and relatively coarse Widmanstätten  $\alpha$ , which is a  $\beta$  transformation product that forms on characteristic crystallographic planes in the  $\beta$  phase. The Widmanstätten morphology reflects the mechanism of formation of primary  $\alpha$  during cooling of  $\beta$ , and therefore, its appearance during FSP reflects heating to relatively high temperatures ( $>900$  °C), with formation of large volume fractions of  $\beta$ , followed transformation of the  $\beta$  during subsequent cooling at moderate rates. The retention of large fractions of primary  $\alpha$  at lower heating temperatures during FSP apparently precludes the development of the Widmanstätten morphology during subsequent cooling. Figure 3(b) is from a location further below the surface, region 2 in Figure 1(b), and shows a banded structure consisting of primary  $\alpha$  and  $\beta$  phase transformation products similar to those observed in FSP 514. Figure 3(c) is at about the middle of the stir zone and is located in a region that exhibits the onion ring pattern at lower magnification (region 3 in Figure 1(b)). At this higher magnification, the onion ring pattern is seen to consist of bands of fine, equiaxed grains of the  $\alpha$  phase that are surrounded by transformation products of the  $\beta$ , while the rings reflect periodic variations in both the volume fraction of  $\beta$  transformation products and the grain size. Below the stir zone, grain deformation in the microstructure in Figure 3(d) suggests material flow due to tool rotation (region 4 in Figure 1(b)). Material in this region exhibits much finer grains (to be further discussed in Section B), although the grains are indistinct in this optical micrograph. Transformation products of the  $\beta$  phase are not apparent in this region.

The FSP 528 sample also exhibits Widmanstätten  $\alpha$  in the upper regions of the stir zone (region 1 in Figure 1(c)), as shown in Figure 4(a). A mixture of fine Widmanstätten  $\alpha$  and fine, equiaxed  $\alpha$  grains is apparent at the middle of the stir zone, as shown in Figure 4(b); this is the onion-ring region (region 2 in Figure 1(c)) that is distinct at the middle of the stir zone of FSP 528. The volume fraction of  $\beta$  transformation products is larger in bands containing Widmanstätten  $\alpha$  and smaller in adjacent regions containing mostly equiaxed  $\alpha$ . In Figure 4(c), a very fine mixture of elongated primary  $\alpha$  grains and elongated products of  $\beta$  transformation is apparent at the region nearest the bottom of the stir zone (region 3 in Figure 1(c)). The direction of elongation is horizontal.

Widmanstätten  $\alpha$  was observed mainly in the upper regions of the FSP 520 and FSP 528 samples, and no Widmanstätten  $\alpha$  is apparent in FSP 514. The presence of this transformation product indicates nearly complete transformation to the  $\beta$  phase at the local peak temperature attained during the FSP thermomechanical cycle. In turn, this result suggests that the local peak temperature in near-surface regions is higher in FSP 520 and 528 when compared to that attained in FSP 514. Nevertheless, from the present OM observations, the  $\kappa_{ii}$  is apparent throughout the stir zone in all of these samples, and this suggests incomplete re-dissolution of  $\kappa_{ii}$  in the  $\beta$  despite local peak temperature that may exceed 930 °C (which is the  $\kappa_{ii}$  solvus temperature for the nominal alloy composition).

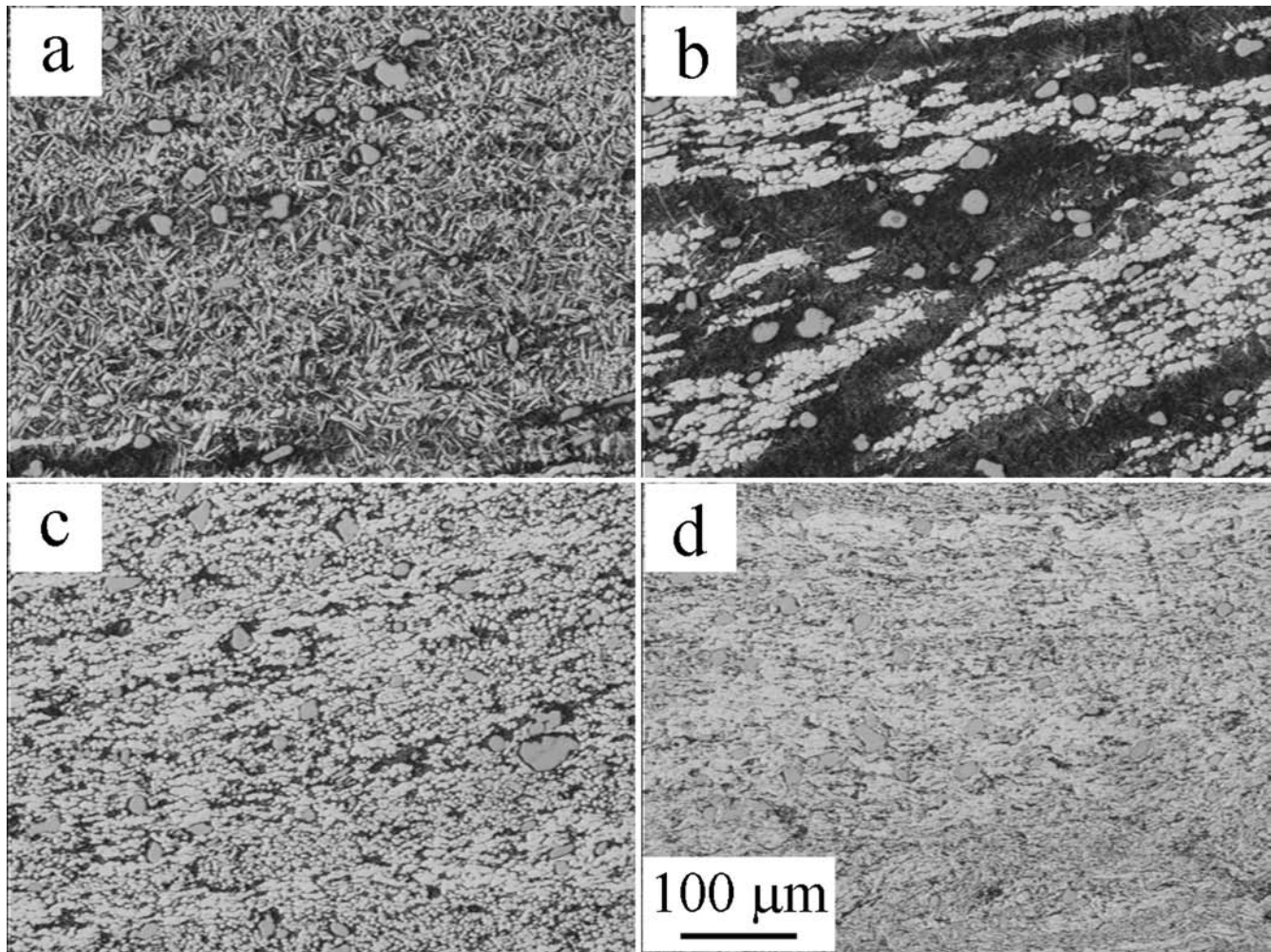


Fig. 3—A series of higher magnification optical micrographs from regions 1 to 4 along a traverse through the center of the stir zone in FSP 520. (a) through (d) Micrographs corresponding to regions 1 through 4, respectively, in Fig. 1(b).

### B. Microstructure Examination by TEM

Thin foils for TEM examination were also prepared from this sample set for further analysis of the effect of FSP parameters on the evolution of microstructure. Figure 5 shows TEM micrographs from the upper region of FSP 514. This region contains mainly elongated primary  $\alpha$  and  $\beta$  transformation products, as shown in Figures 1(a) and 2, and the data of Figure 5 correspond to a specific location that is in the prior  $\beta$ . Figure 5(a) is a BF image and selected area diffraction (SAD) pattern, and Figure 5(b) is a dark-field (DF) image, from the same position. Fine features that have formed along characteristic directions as well as fine globular particles are apparent in these images. Many spots are apparent in the SAD pattern, which had been obtained with a  $\sim 1 \mu\text{m}$  aperture, reflecting the presence of more than one crystal orientation. The DF image taken by spot B in the SAD pattern highlights one variant of a martensitic transformation product. This microstructure is similar to the martensite described by Hasan *et al.*<sup>[19]</sup> in an investigation of transformations in this alloy system. Such a phase does not exist in the as-cast condition of this material, and so this constituent has formed by transformation of  $\beta$  during rapid cooling in the thermomechanical cycle of the FSP.

Figure 6 consists of TEM micrographs showing globular particles and lamellar-appearing precipitates at a location adjacent to that of the martensite shown in Figure 5. Figure 6(a) is the BF image, while Figures 6(b) and (c) are the DF images obtained from spots B and C, respectively. By calculation of lattice spacing for each spot in the SAD pattern, spot B arises from both the B2 and the  $\text{DO}_3$  structure types, while spot C comes from only the  $\text{DO}_3$  structure type. A fully ordered  $\text{Fe}_3\text{Al}$  phase (*i.e.*, the  $\kappa_{ii}$  and the  $\kappa_{iv}$ ) having the  $\text{DO}_3$  structure and a fully ordered NiAl phase (*i.e.*, the  $\kappa_{iii}$ ) having the B2 structure will have interatom spacings that differ by less than 1 pct and therefore will exhibit similar electron diffraction patterns. Nevertheless, these phases can be distinguished with selected spots in the SAD pattern, *e.g.*,  $111_{\text{DO}_3}$ ,  $113_{\text{DO}_3}$ . Thus, in Figure 6(b), both the globular particles and lamellar-appearing particles are bright, while in Figure 6(c), only central regions of the globular particles are light. This indicates that central regions of the globular particles are the  $\text{DO}_3$  phase, while the outer layer is the B2 phase, and so the globular particles are composite precipitates. Such composite precipitates are also consistent with the results of Hasan *et al.*<sup>[19,21]</sup> There are also light areas in Figure 6(c) away from the core of the globular particles. Swann and Warlimont<sup>[27]</sup> have shown

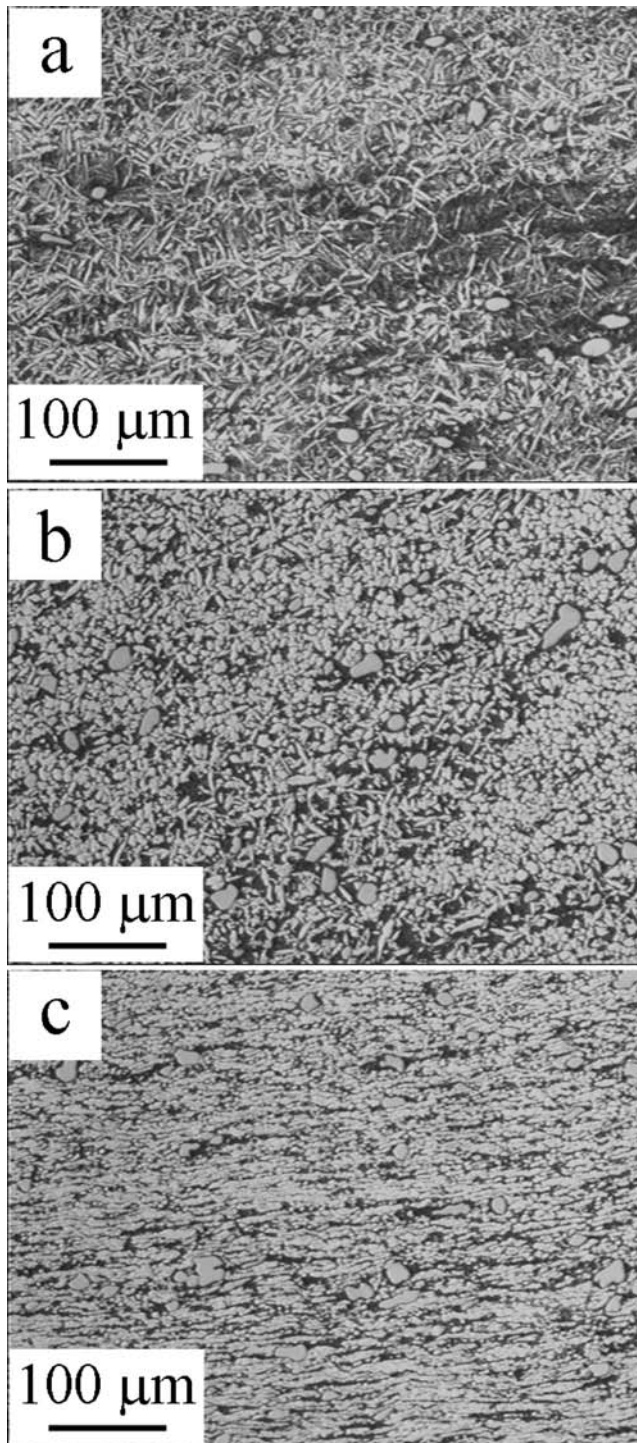


Fig. 4—A series of higher magnification optical micrographs from a traverse through the center of the stir zone in FSP 528. (a) through (c) Micrographs corresponding to regions 1 to 3, respectively, in Fig. 1(c).

that there are three types of martensite in Cu-Al binary alloys: (1) a distorted fcc type,  $\beta'$ ; (2) a tetragonal, ordered type,  $\beta_1'$ ; and (3) an ordered hcp type,  $\gamma'$ . The martensite phases are denoted  $\beta'$  in binary alloys that have <11 pct Al,  $\beta_1'$  for 11 to 13 pct Al, and  $\gamma'$  for >13 pct Al. Furthermore, in alloys containing >11 pct Al, the high-temperature bcc  $\beta$  phase transforms to an ordered  $\beta_1$  having a  $DO_3$  structure prior to

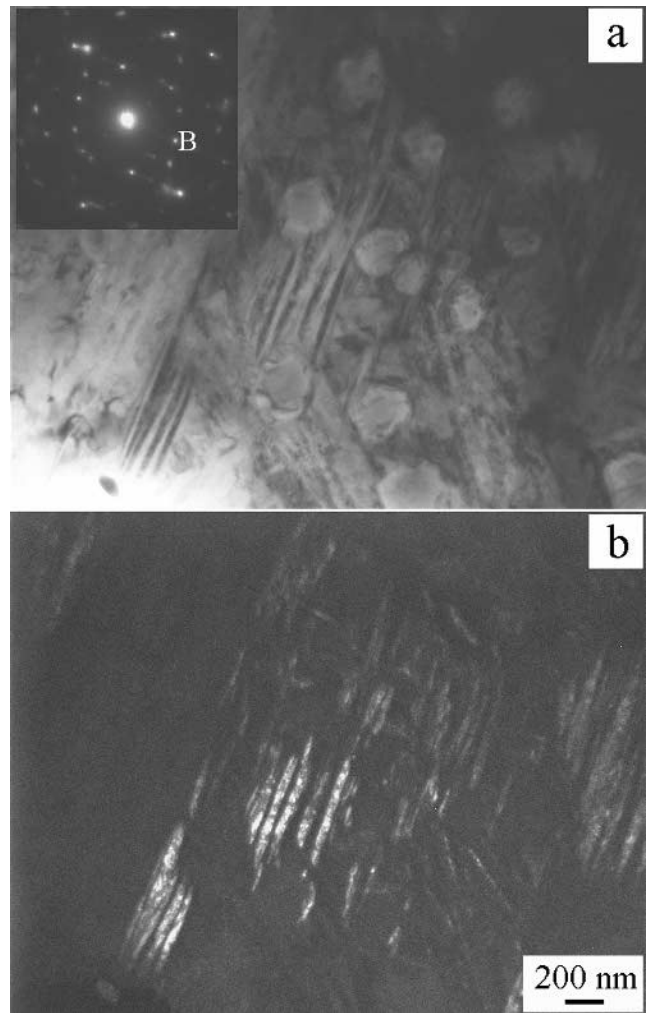


Fig. 5—TEM micrographs from a location near region 1 in FSP 514; corresponding OM data are shown in Figs. 1(a) and 2(a). (a) BF image and (b) DF image taken using spot B in the SAD pattern; the microstructure is martensitic with globular particles.

the martensite transformation, and then transforms martensitically to either  $\beta_1'$  or  $\gamma'$ . This suggests the possibility that the  $\beta$  phase in the alloy of this investigation may have transformed to  $Fe_3Al$  having  $DO_3$  structure type before the occurrence of the martensite transformation, and so the martensite would be expected to be  $\beta_1'$  or  $\gamma'$ .

Figure 7 shows the microstructure from the lower region in FSP 514. Coarser particles having an ellipsoidal shape and martensitic transformation products formed in areas nearby the particles are apparent in Figure 7(a). This martensite comprises fine variants that align alternately along characteristic directions. The particles exhibited larger amounts of Fe and small amounts of Al by energy-dispersive spectrometry analysis, and so they are expected to be the  $Fe_3Al$  phase (*i.e.*,  $\kappa_{ii}$  or  $\kappa_{iv}$ ) that has been broken up and spheroidized by severe deformation during FSP. The formation of martensite nearby these particles indicates that the concentrations of Al, Ni, and Fe are enriched in the immediate vicinity of the particles due to partial dissolution of  $\kappa_{ii}$  during FSP. Figures 7(b) and (c) show globular and lamellar-appearing precipitates also located near the martensite; Figure 7(c) is a DF image acquired using

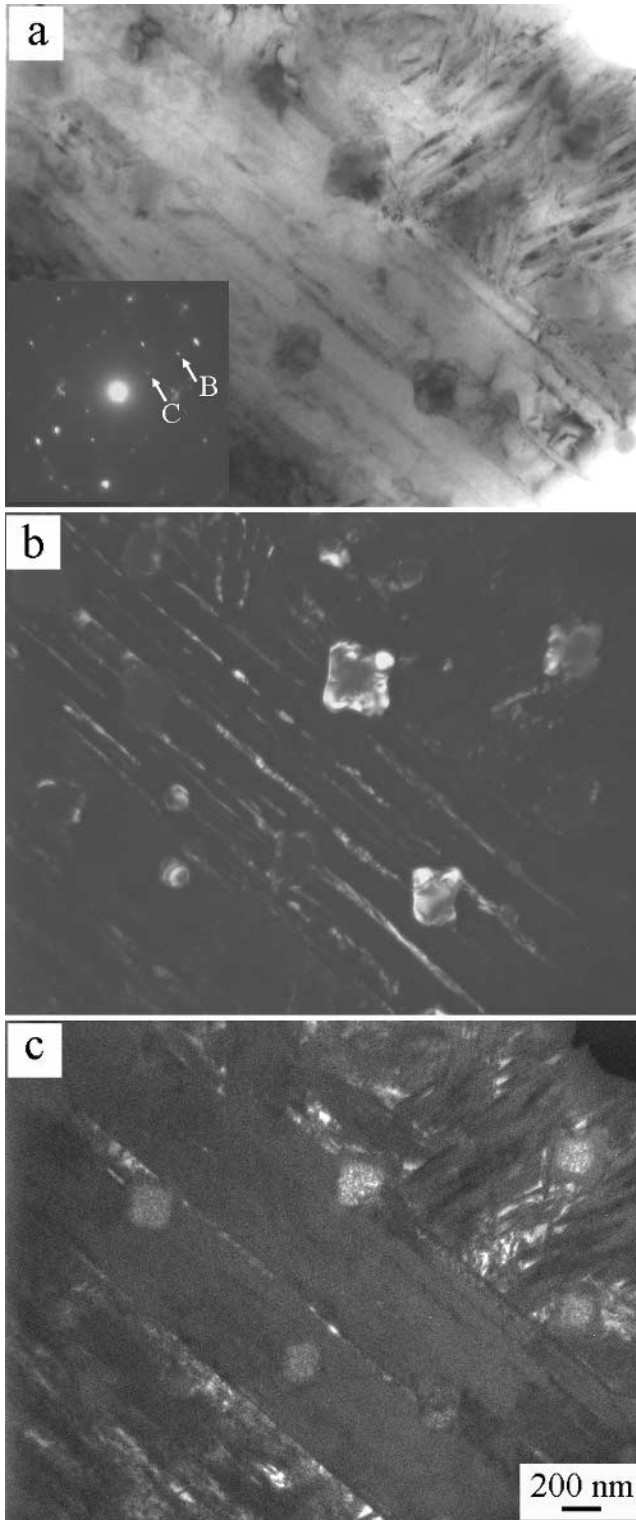


Fig. 6—(a) Micrograph of the BF image. (b) and (c) The DF images taken using spots B and C in the SAD pattern, respectively, and showing lamellar particles and composite precipitates consisting of a  $DO_3$  phase core with a  $B_2$  phase outer layer.

the  $100_{B_2}$  spot in the SAD pattern of Figure 7(b). Both the globular and lamellar-appearing precipitates are larger when compared to the corresponding precipitates in the upper region of this sample. The globular particles are, again, composite

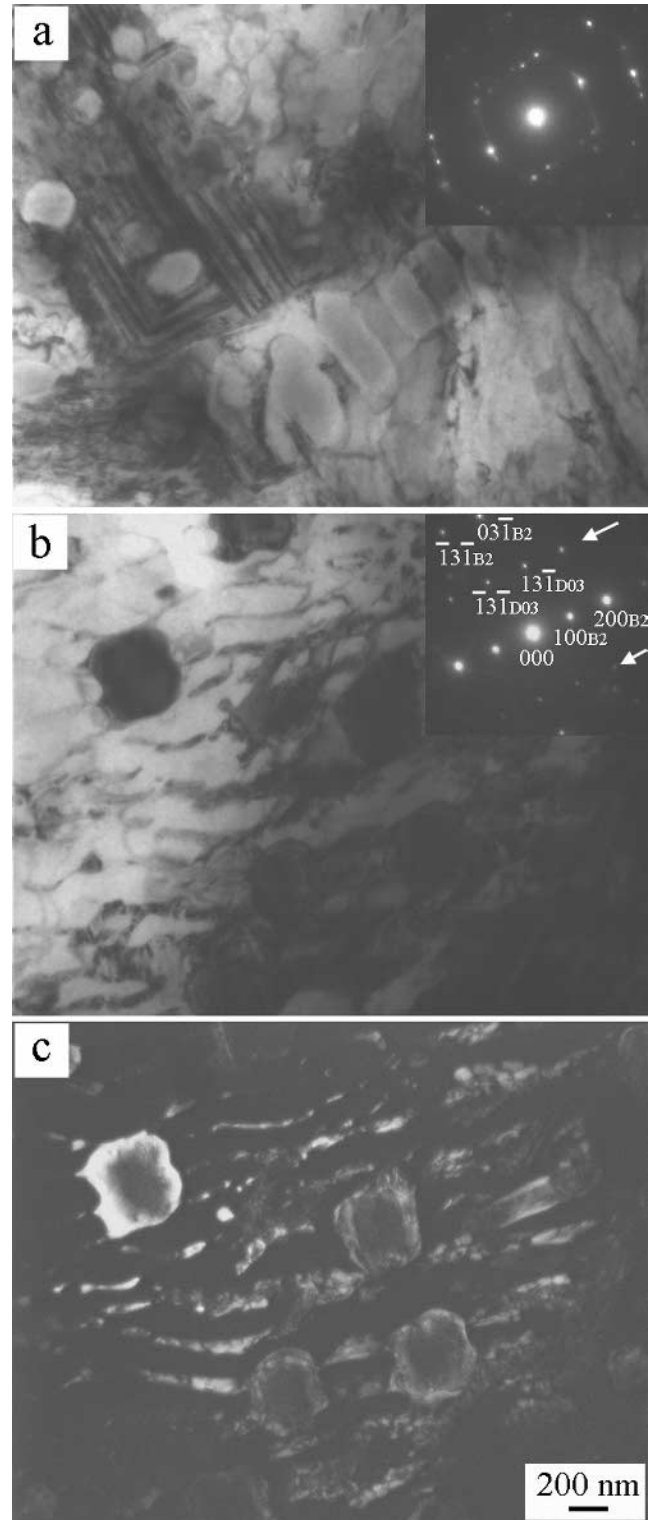


Fig. 7—TEM micrographs from a location near region 2 in FSP 514; corresponding OM data are shown in Figs. 1(a) and 2(b). (a) BF image showing coarser particles and martensitic transformation products formed around the particles. (b) and (c) Lamellar-appearing and globular precipitates formed in the vicinity of the martensite shown in (a).

precipitates, as seen in the upper region, because the additional spots indicated by the arrows in the SAD pattern are due to the  $DO_3$  structure type. The lamellar particles appear

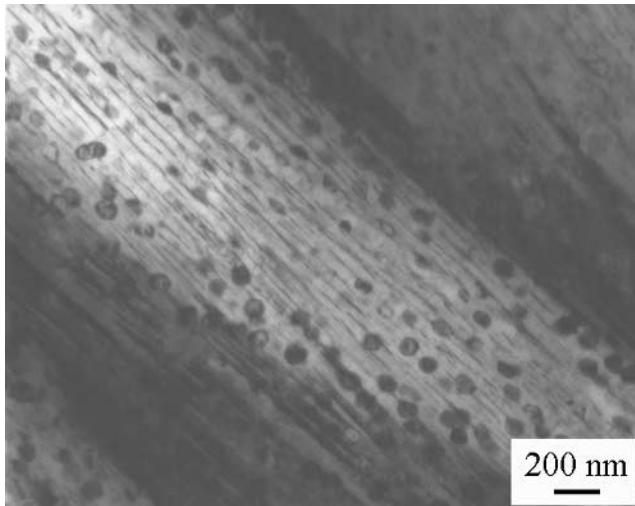


Fig. 8—A TEM micrograph from a location near region 2 in FSP 520, as shown previously in Figs. 1(b) and 3(b), illustrating lamellar-appearing and globular particles. The sizes of the particles are much smaller than those in FSP 514 (Figs. 6 and 7).

to be separated by darker boundaries. This suggests that the region experienced high temperatures for a sufficient time and that the particles have grown and become surrounded by misfit dislocations. In FSP 514 mixed structures, martensite and bainite are observed not only in the upper region but also in the lower region. This is consistent with OM observations.

Figure 8 is a TEM micrograph obtained in FSP 520 from a location near region 2 in Figure 1(b). This image shows lamellar-appearing particles and globular precipitates. A comparison of the image in Figure 8 with the images in Figures 6 and 7 reveals that the lamellar-appearing and globular particles are much finer than those in FSP 514. The globular particles have either the B2 or the DO<sub>3</sub> structure, but identification of a composite precipitate structure, such as that observed in the FSP 514 material, was not feasible. Again, martensite was observed nearby this location. A mixed structure of bainite, martensite, and fine globular particles was observed even in the middle of the stir zone in FSP 528. Thus, the microstructures with dark etching constituents consisting of these  $\beta$  transformation products in OM are consistent with TEM results in all samples.

Figure 9 is a histogram summarizing the variation in sizes, determined from TEM micrographs, of the globular particles and the spacing of the lamellar particles in the bainite from each of the conditions given in Table II. These data were all acquired from regions exhibiting elongated and banded mixtures of primary  $\alpha$  and transformation products of  $\beta$ . Such microstructures reflect heating to temperatures of  $\sim 900$  °C and were apparent throughout FSP 514, while they were only seen in limited regions of FSP 516, 520, and 528. Both the globular particle size and lamellar spacing are largest in FSP 514. The globular particle size appears to increase with depth along the center of the stir zone, while the spacing of the lamellar particles remains constant within the error of measurement. For all other processing conditions, the globular particle sizes and lamellar spacing values are smaller than for FSP 514 and, furthermore, are identical for FSP 516, 520, and 528 within measurement error. The larger globular particle size in FSP 514 may reflect slower cooling due to the larger volume of the stir

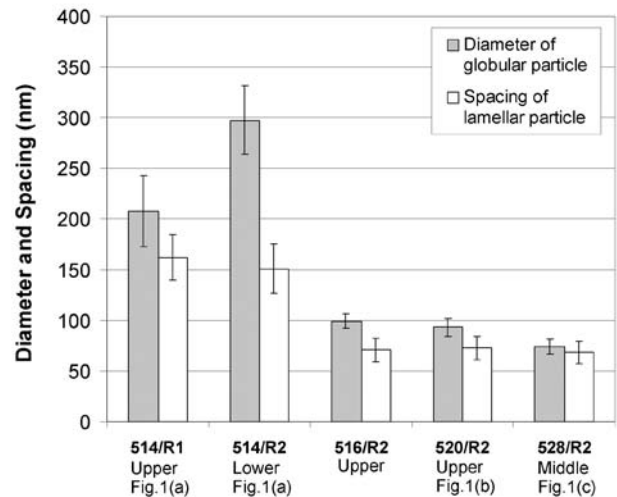


Fig. 9—A histogram illustrating the variation in sizes of globular particles and the spacing of lamella in the  $\beta$  transformation products obtained from TEM micrographs in regions exhibiting elongated and banded mixtures of primary  $\alpha$  and  $\beta$  transformation products.

zone for this condition, and thus more time for growth following nucleation. However, it is also possible that the  $\kappa_{iii}$  portion of these particles formed on either  $\kappa_{ii}$  or  $\kappa_{iv}$  particles that did not dissolve but instead were deformed and broken up by FSP. Such particles would not have formed directly from the  $\beta$  phase, and this may account for the large size of such particles in the lower portion of the stir zone of FSP 514. The fine lamellar particles form from the  $\beta$  by bainitic transformation during the cooling part of the FSP thermomechanical cycle. The reduction in spacing observed in Figure 9 corresponds with the reduced cross-sectional areas of the stir zones (Figure 1), which, in turn, reflects increased cooling rates from 900 °C.

Figure 10(a) is a representative microstructure of the elongated primary  $\alpha$  located within the band structure in the upper region 2 of FSP 520. This corresponds to the light area in region 2 that was shown in Figures 1(b) and 3(b). This image shows an annealing twin as well as substructure, reflecting deformation, recovery, and, possibly, recrystallization in the primary  $\alpha$  during the FSP thermomechanical cycle. Such an  $\alpha$  phase microstructure was common for regions in all samples that exhibited bandlike structures. Figure 10(b) is a representative microstructure from the lower region 4 of FSP 520 (Figures 1(b) and 3(d)), and shows a highly refined  $\alpha$  grain 1 to 2  $\mu\text{m}$  in size. Annealing twins are evident in the  $\alpha$  phase grain boundaries rather than the  $\beta$  transformation products evident in the upper region of this sample. Regions near grain boundary triple junctions may include particles from the eutectoid constituent in the as-cast conditions that have been broken by FSP. This microstructure is essentially identical to that reported previously for FSP 516<sup>[16]</sup> and may reflect recrystallization by particle-stimulated nucleation<sup>[28,29]</sup> of recrystallization and grain growth that is restricted by fine precipitates.

#### IV. DISCUSSION

Stir zone microstructures and their spatial variation depend upon FSP parameters. For the tools employed in this study,

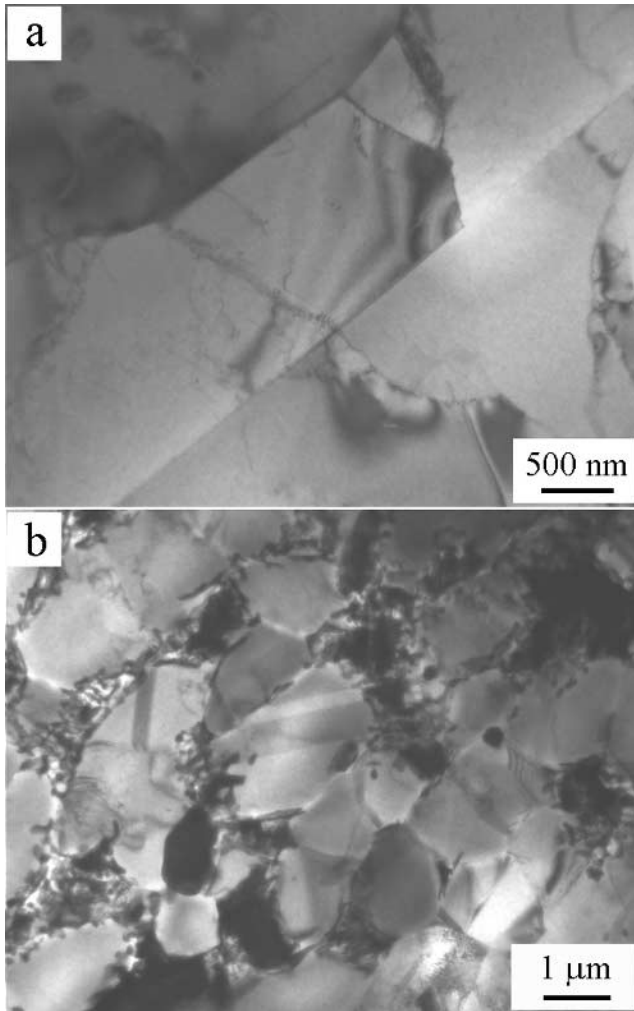


Fig. 10—(a) TEM micrograph of the elongated primary  $\alpha$  located within the band structure in the upper region 2 of FSP 520, illustrating annealing twins as well as deformation-induced substructure. (b) TEM micrograph from the lower region 4 of FSP 520 showing a refined  $\alpha$  grain structure with fine particles along the  $\alpha$  boundaries as well as clusters of irregularly shaped particles in the vicinity of grain triple junctions.

processing at low rotation and traversing rates (*i.e.*, FSP 514) resulted in relatively uniform microstructures throughout the stir zone, while processing at high tool rotation and traversing rates (*i.e.*, FSP 528) resulted in distinct gradients in the stir zone microstructure. Thus, FSP parameters affect peak temperatures, times at temperature, subsequent cooling rates, and strain and strain rate throughout the stir zone, and adjacent locations in the stir zone microstructure may experience distinctly different thermomechanical histories.

Predictive models of the thermomechanical cycle throughout the stir zone as well as its dependence on FSP parameters remain to be established. Nevertheless, detailed analysis of stir zone and TMAZ microstructures in NAB materials has provided a method to estimate local peak temperatures due to FSP.<sup>[16]</sup> These estimates assume that cooling rates following FSP are much greater than those in equilibrium-cooled as-cast material. Thus, in as-cast NAB having the nominal UNS95800 composition, the lamellar  $\alpha + \kappa_{iii}$  will begin to transform to  $\beta$  as the local temperature reaches  $\sim 800^\circ\text{C}$  and the fraction of  $\beta$  will increase with further

heating above this temperature. The  $\kappa_{iv}$  phase will begin to dissolve into the remaining primary  $\alpha$  beginning at  $\sim 860^\circ\text{C}$ , while the  $\kappa_{ii}$  phase will dissolve into the  $\beta$  beginning at  $\sim 930^\circ\text{C}$ . At  $\sim 1030^\circ\text{C}$ , the microstructure will become entirely  $\beta$ . These transformations on heating will be accelerated significantly by the concurrent deformation of the material.<sup>[30,31,32]</sup> Various cooling transformations will occur following passage of the tool, and the transformation products will depend on the prior local peak temperature as well as the subsequent cooling rate. For locations that have experienced heating to near  $1000^\circ\text{C}$ , and therefore the formation of large  $\beta$  volume fractions during straining and heating, subsequent cooling at rates typical of FSP will result in the successive formation of, first, Widmanstätten  $\alpha$ , then bainite, and, finally, martensite. At locations that have experienced straining with heating to lower temperatures, resulting in mixtures of untransformed primary  $\alpha$  as well as  $\beta$ , the resulting microstructure will comprise the primary  $\alpha$  and various transformation products of the  $\beta$ . The latter will include, again, Widmanstätten  $\alpha$ , bainite, and martensite.

Figure 11 shows schematic stir zone thermal cycles based on microstructure analysis for the different FSP conditions of this investigation. The calculated ratio of traversing rate to rotation rate, *i.e.*, millimeter of tool advance per revolution of the tool, is provided in Figure 11 for each of these FSP processes. This ratio varies from 0.04 mm/rev for FSP 514, the slowest process, to 0.34 mm/rev for FSP 528, the fastest process. Altogether, three differences among the microstructures of the materials of this investigation are related to processing speed: (1) morphology of the primary  $\alpha$ , (2) development of the Widmanstätten  $\alpha$ , and (3) formation of the “onion ring” structure in the mid regions of faster processes. Furthermore, these differences are associated with features that are much smaller in scale than the sizes of the stir zones.

For the slowest process (FSP 514), the microstructure throughout the stir zone consists of elongated and banded grains of the primary  $\alpha$  and transformation products of the  $\beta$  phase. Such microstructures reflect severe deformation near the midpoint in temperature of the  $\alpha + \beta$  two-phase region of the phase diagram. From analysis of the relative fractions of primary  $\alpha$  and  $\beta$ , the peak temperature near the surface in contact with the tool is  $\sim 920^\circ\text{C}$  while that at the bottom of the stir zone is  $\sim 850^\circ\text{C}$ . The primary  $\alpha$  grain size is coarser in FSP 514 than it is for similar microstructures produced by the other processes. Furthermore, the sizes of the globular particles and spacings of the lamellar particles in the  $\beta$  transformation products (Figure 9) are both largest in FSP 514.

As processes become faster, the depth of the stir zone decreases while the microstructure data indicate that temperature differences in the stir zone become greater; together, these factors suggest steeper temperature gradients in the stir zone. The presence of Widmanstätten  $\alpha$  near the surface in contact with the tool reflects an increase in temperature at this location, while temperatures at the bottom of the stir zone apparently decrease toward the temperature for the eutectoid reversion reaction  $\alpha + \kappa_{iii} \rightarrow \beta$ . The appearance of Widmanstätten  $\alpha$  near the surface in contact with the tool indicates that peak temperatures are approaching  $\sim 1030^\circ\text{C}$  in FSP 520 and 528; there was less of the Widmanstätten  $\alpha$  constituent in FSP 516, and this is consistent with a somewhat lower peak temperature for this processing condition

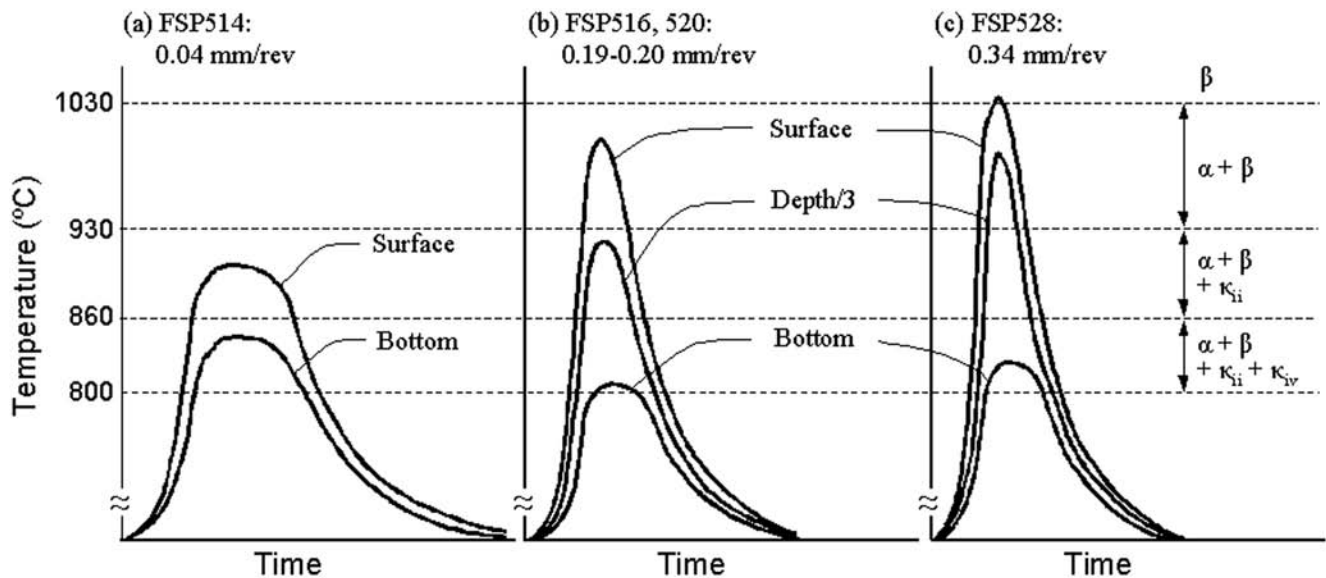


Fig. 11—Schematics of stir zone thermal cycles are illustrated for the processing conditions examined in this study. The peak temperatures of these cycles are based on microstructure observations of these samples.

despite a ratio of traversing rate to rotation rate that is nominally the same as that for the FSP 520 condition. Widmanstätten  $\alpha$  forms from  $\beta$  at moderate to low cooling rate and the amount of this constituent apparently depends on solute content and undercooling. Studies of annealing and either quenching or air cooling of the as-cast NAB material have shown that high cooling rates ( $\sim 10^{+3} \text{ }^\circ\text{C s}^{-1}$ ) suppress the formation of Widmanstätten  $\alpha$  for any annealing temperature in the  $\alpha + \beta$  range of the phase diagram.<sup>[33]</sup> This constituent forms from the  $\beta$  at moderate cooling rates ( $\sim 10^0 \text{ }^\circ\text{C s}^{-1}$ ) but the amount decreases as the annealing temperature decreases, and the Widmanstätten morphology is no longer apparent below an annealing temperature of about  $900 \text{ }^\circ\text{C}$ . This may reflect an increased solute content in the  $\beta$  as annealing temperature is decreased and a greater tendency for bainitic or martensitic transformation upon subsequent cooling. On this basis, the near-surface regions in FSP 520 and 528 attained temperatures  $\sim 1030 \text{ }^\circ\text{C}$  with complete transformation to  $\beta$ , followed by  $\alpha$  phase formation with the Widmanstätten morphology as well as bainite and martensite.

An increased tendency for spheroidization of the microstructure constituents was apparent at higher processing speeds. For example, comparison of the banded structures among the different processes reveals that the primary  $\alpha$  grains are more nearly equiaxed in fast processes than in slow processes. This reflects the severe straining in the FSP thermomechanical cycle. Also, while the  $\kappa_{iv}$  and  $\kappa_{ii}$  are both nominally  $\text{Fe}_3\text{Al}$  having a  $\text{D0}_3$  structure, the  $\kappa_{iv}$  may dissolve more readily than the  $\kappa_{ii}$  because it is finer in size, which is, in turn, a reflection of its lower solvus temperature of  $\sim 860 \text{ }^\circ\text{C}$ . The severe straining of FSP may also induce recrystallization in the primary  $\alpha$  at undissolved  $\kappa_{iv}$  particles, or in association with  $\beta$  phase formed in the primary  $\alpha$  by dissolution of the  $\kappa_{iv}$  upon heating above the  $\kappa_{iv}$  solvus temperature. At higher stir zone temperatures, the remaining primary  $\alpha$  may have a similar role in recrystallization of the

$\beta$  insofar as the bcc  $\beta$  should be softer at temperature than the fcc  $\alpha$ .

Complex material flow patterns, *i.e.*, onion rings are evident below the banded regions in FSP 520 and 528, as indicated in Figures 3(c) and 4(b). The onion rings comprise two kinds of microstructure. In FSP 520 (Figure 3(c)), each ringlike band consists of layers of elongated  $\alpha$  grains and equiaxed  $\alpha$  grains, surrounded by fine  $\beta$  phase transformation products. In the faster FSP 528 process (Figure 4(b)), the onion rings consist of spheroidized  $\alpha$  and Widmanstätten  $\alpha$  layers; the latter layer also contains a large volume fraction of other, fine  $\beta$  transformation products. Such onion ring structures reflect complex strain histories in the stir zone and have been reported in Al alloys processed by FSW as well as FSP.<sup>[3,12-15]</sup> In general, the ring spacing in planes parallel to the direction of tool motion corresponds to the ratio of tool advance per revolution.<sup>[14,26]</sup> In AA2024 and 2524 alloys, onion ring structures involving alternating bands of finer and coarser grains have been reported.<sup>[12-15]</sup> The size and distribution of constituent particles as well as the microhardness also differ along with the grain size. Predictive models for the onion ring structure have not been developed. In the present study, one band has a larger volume fraction of  $\beta$  transformation products than the adjacent band, and this suggests that the band exhibiting the larger volume fraction of  $\beta$  experienced a higher peak temperature in its strain history. Short-range periodic variations in temperature are unlikely, and so this result suggests that the material of adjacent bands moved from different initial locations and therefore experienced different thermal histories.

The  $\kappa_{ii}$  phase was present in all samples even though local peak temperatures apparently attained values above the solvus temperature,  $930 \text{ }^\circ\text{C}$ , for this phase. Such peak temperatures were only attained in the faster processes. In a previous investigation, prolonged heating was necessary to dissolve the coarse  $\kappa_{ii}$  particles.<sup>[33]</sup> These particles are generally  $>20 \mu\text{m}$

in size and they persisted during 6 minutes of annealing at 950 °C, although they were completely dissolved after 1 hour at this temperature. In contrast, the equilibrium fraction of  $\beta$  was attained in 6 minutes at this temperature. The  $\kappa_{ii}$  (Fe<sub>3</sub>Al) is an ordered phase having Fe as its major component. The solute diffusion coefficients for Al, Fe, and Ni in Cu at 900 °C are  $2.14 \times 10^{-9} \text{ cm}^2 \text{ s}^{-1}$ ,<sup>[34]</sup>  $3.00 \times 10^{-10} \text{ cm}^2 \text{ s}^{-1}$ ,<sup>[35]</sup> and  $7.74 \times 10^{-11} \text{ cm}^2 \text{ s}^{-1}$ ,<sup>[35]</sup> respectively. The self-diffusion coefficient for Cu is  $3.20 \times 10^{-10} \text{ cm}^2 \text{ s}^{-1}$ ,<sup>[35]</sup> almost the same as that for Fe. The diffusion coefficients for Fe and Ni solutes as well as the self-diffusion coefficient for Cu are all smaller than that the Al diffusion coefficient. Thus, during the brief heating of the faster FSP processes, the  $\kappa_{ii}$  may persist at temperatures above its solvus.

## V. CONCLUSIONS

1. For the tool and processing conditions of this investigation, uniform microstructures and relatively flat temperature distributions are inferred at low tool rotation and travel rates.
2. Stir zone depth decreases as tool rotation and travel rates increase, especially under the tool shoulder; decreasing stir zone depth under the tool pin reflects compressive deformation of the tool pin as well as shallower penetration of the deformation and heating of FSP.
3. The onion ring structure, which reflects complex material flow patterns involving displacements parallel to as well as perpendicular to the tool axis, is formed at higher rotation and travel rates.
4. The development of coarse Widmanstätten  $\alpha$  indicates that the local peak temperature during FSP is  $\sim 1030$  °C, *i.e.*, within the single-phase  $\beta$  region in the phase diagram, and that the subsequent cooling rate is moderate.
5. Maximum peak temperatures during FSP are estimated to be higher for high tool rotation rates, *i.e.*, in the order  $\text{FSP } 514 < \text{FSP } 516 < \text{FSP } 520 < \text{FSP } 528$ .
6. Spheroidization of microstructure is attributed to severe local deformation during FSP.
7. Retention of the  $\kappa_{ii}$  phase throughout all stir zones in this investigation suggests that time at temperature is insufficient for complete dissolution of this constituent into the  $\beta$  phase.

## ACKNOWLEDGMENTS

The authors acknowledge the provision of FSP materials by Mr. Murray Mahoney, Rockwell Scientific Corporation. The Naval Surface Warfare Center (Carderock, MD) supplied the NAB material, and the Defense Advanced Research Projects Agency (DARPA), with Dr. Leo Christodolou as program sponsor, provided funding for this work. We are grateful to Mr. Yuichi Miyahara, Kyushu University, for helping with the ion milling.

## REFERENCES

1. R.S. Mishra: *Adv. Mater. Processes*, 2003, vol. 161 (10), pp. 43-46.
2. R.S. Mishra, Z.Y. Ma, and I. Charit: *Mater. Sci. Eng. A*, 2003, vol. A341, pp. 307-10.
3. Z.Y. Ma, R.S. Mishra, and M.W. Mahoney: in *Friction Stir Welding and Processing II*, K.V. Jata, M.W. Mahoney, R.S. Mishra, S.L. Semiatin, and T. Lienert, eds., TMS, Warrendale, PA, 2003, pp. 221-30.
4. R.S. Mishra, M.W. Mahoney, S.X. McFadden, N.A. Mara, and A.K. Mukherjee: *Scripta Mater.*, 2000, vol. 42, pp. 163-68.
5. R.S. Mishra and M.W. Mahoney: in *Superplasticity in Advanced Materials—Proc. ICSAM2000*, N. Chandra, ed., Materials Science Forum, Trans Tech Publications, Aedermannsdorf, Switzerland, 2001, vols. 357-359, pp. 507-14.
6. Z.Y. Ma, R.S. Mishra, and M.W. Mahoney: *Acta Mater.*, 2002, vol. 50, pp. 4419-30.
7. P.B. Berbon, W.H. Bingel, R.S. Mishra, C.C. Bampton, and M.W. Mahoney: *Scripta Mater.*, 2001, vol. 44, pp. 61-66.
8. I. Charit and R.S. Mishra: *Mater. Sci. Eng. A*, 2003, vol. A359, pp. 290-96.
9. Z.Y. Ma, R.S. Mishra, M.W. Mahoney, and R. Grimes: *Mater. Sci. Eng. A*, 2003, vol. A351, pp. 148-53.
10. Y.S. Sato, M. Urata, and H. Kokawa: *Metall. Mater. Trans. A*, 2002, vol. 33A, p. 625-35.
11. H.S. Park, T. Kimura, T. Murakami, Y. Nagano, K. Nakata, and M. Ushio: *Mater. Sci. Eng. A*, 2004, vol. A371, pp. 160-69.
12. M.A. Sutton, B. Yang, A.P. Reynolds, and R. Taylor: *Mater. Sci. Eng. A*, 2002, vol. A323, pp. 160-66.
13. M.A. Sutton, A.P. Reynolds, B. Yang, and R. Taylor: *Mater. Sci. Eng. A*, 2003, vol. A354, pp. 6-16.
14. B. Yang, J. Yan, M.A. Sutton, and A.P. Reynolds: *Mater. Sci. Eng. A*, 2004, vol. A364, pp. 55-65.
15. M.A. Sutton, B. Yang, A.P. Reynolds, and J. Yan: *Mater. Sci. Eng. A*, 2004, vol. A364, pp. 66-74.
16. K. Oh-ishi and T.R. McNelley: *Metall. Mater. Trans. A*, 2004, vol. 35A, pp. 2951-61.
17. P. Brezina: *Int. Met. Rev.*, 1982, vol. 27, pp. 77-120.
18. F. Hasan, A. Jahanafrooz, G.W. Lorimer, and N. Ridley: *Metall. Trans. A*, 1982, vol. 13A, pp. 1337-45.
19. F. Hasan, G.W. Lorimer, and N. Ridley: *J. Phys.*, 1982, vol. 43, pp. C4-653-C4-58.
20. A. Jahanafrooz, F. Hasan, G.W. Lorimer, and N. Ridley: *Metall. Trans. A*, 1983, vol. 14A, pp. 1951-56.
21. F. Hasan, G.W. Lorimer, and N. Ridley: *Met. Sci.*, 1983, vol. 17, pp. 289-95.
22. F. Hasan, J. Iqbal, and N. Ridley: *Mater. Sci. Technol.*, 1985, vol. 1, pp. 312-15.
23. A. Cohen: *Metals Handbook*, 10th ed., ASM INTERNATIONAL, Metals Park, OH, 1990, vol. 2, pp. 386-87.
24. M.W. Mahoney: Rockwell Scientific Company, Thousand Oaks, CA, private communication, 2002.
25. K.N. Krishnan: *Mater. Sci. Eng. A*, 2002, vol. A327, pp. 246-51.
26. T.U. Seidel and A.P. Reynolds: *Metall. Mater. Trans. A*, 2001, vol. 32A, pp. 2879-84.
27. P.R. Swann and H. Warlimont: *Acta Metall.*, 1963, vol. 11, pp. 511-27.
28. F.J. Humphreys: *Acta Metall.*, 1977, vol. 25, pp. 1323-44.
29. R.D. Doherty, D.A. Hughes, F.J. Humphreys, J.J. Jonas, D. Juul-Jensen, M.E. Kassner, W.E. King, T.R. McNelley, H.J. McQueen, and A.D. Rollett: *Mater. Sci. Eng. A*, 1997, vol. A238, pp. 219-74.
30. J.L. Robbins, O.C. Shepard, and O.D. Sherby: *J. Iron Steel Inst.*, 1964, vol. 202, pp. 804-07.
31. O.D. Sherby, B. Walser, C.M. Young, and E.M. Cady: *Scripta Metall.*, 1975, vol. 9, pp. 569-74.
32. B. Walser and O.D. Sherby: *Metall. Trans. A*, 1979, vol. 10A, pp. 1461-71.
33. J. Sherburn: Naval Post Graduate School, Monterey, CA, private communication, 2003.
34. H. Oikawa, T. Obara, and S. Karashima: *Metall. Trans.*, 1970, vol. 1, pp. 2969-70.
35. J. Askill: *Tracer Diffusion Data for Metals, Alloys and Simple Oxides*, IFI Plenum, New York, NY, 1970, pp. 32-45.